a

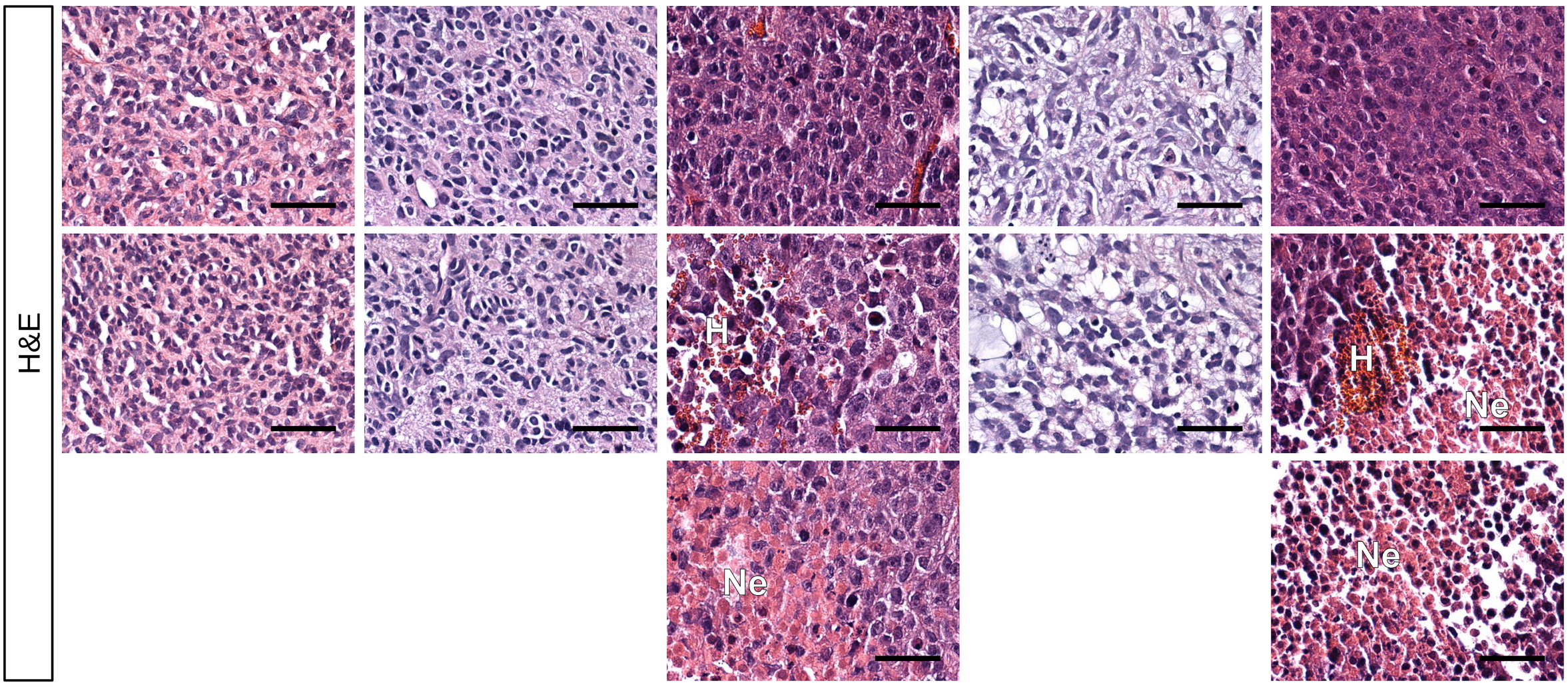

b

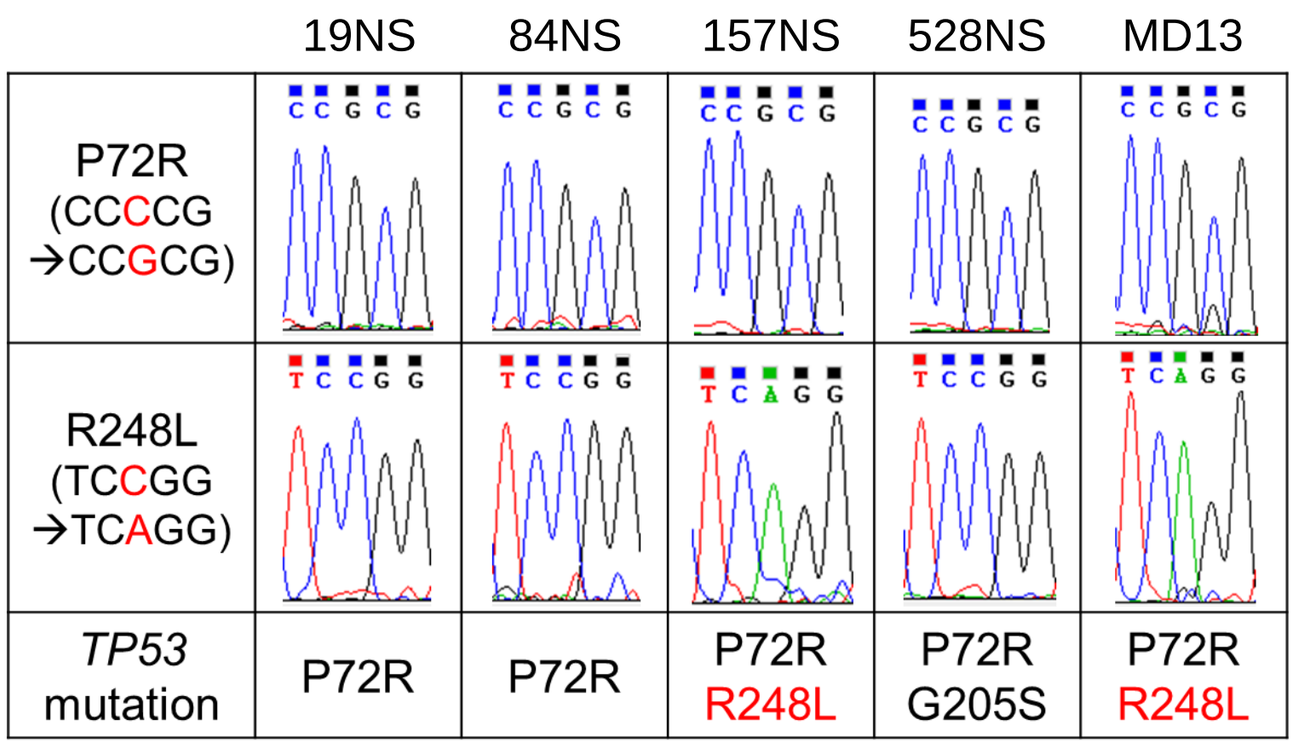

c

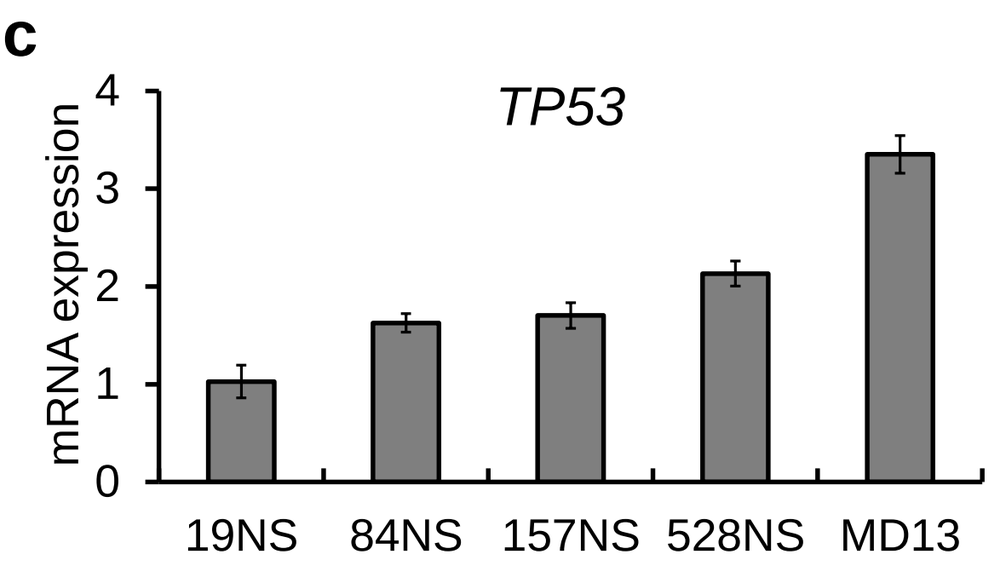

d

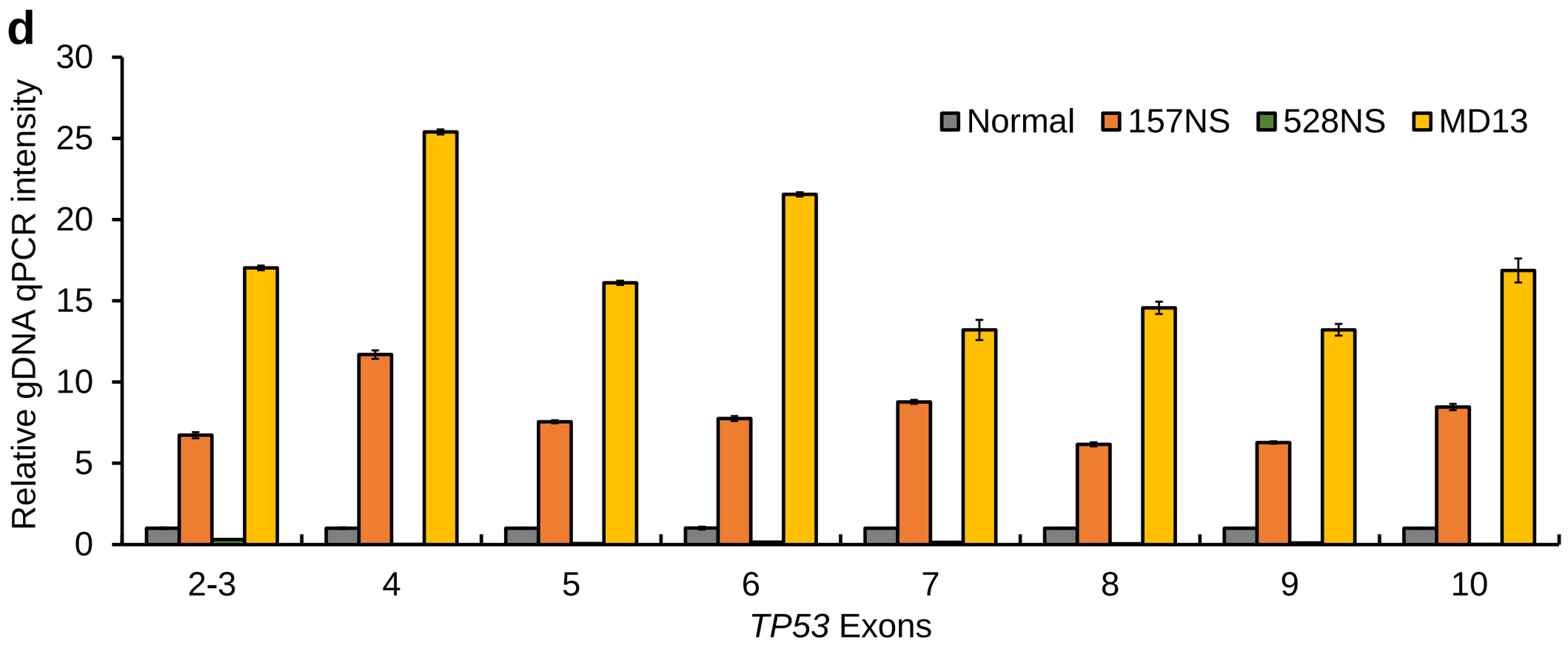

Supplementary Figure S1 Patient-derived GBM xenograft tumors display distinct histological features. (a) Representative microscopic images of H & E staining showing hemorrhage (He) and necrosis (Ne) (magnification 400×, scale bar = 50 μm). (b) Nucleotide substitutions detected by *TP53* coding DNA sequence analysis. (c) qPCR analysis showing *TP53* mRNA level in the patient-derived GBM lines. (d) qPCR analysis to detect the deletion of each exon of *TP53* in the genomic DNA (gDNA). The 157NS and MD13 contained amplified copy number of *TP53*, whereas 528NS apparently harbored a heterozygous deletion. The bar graph represents mean ± SEM.

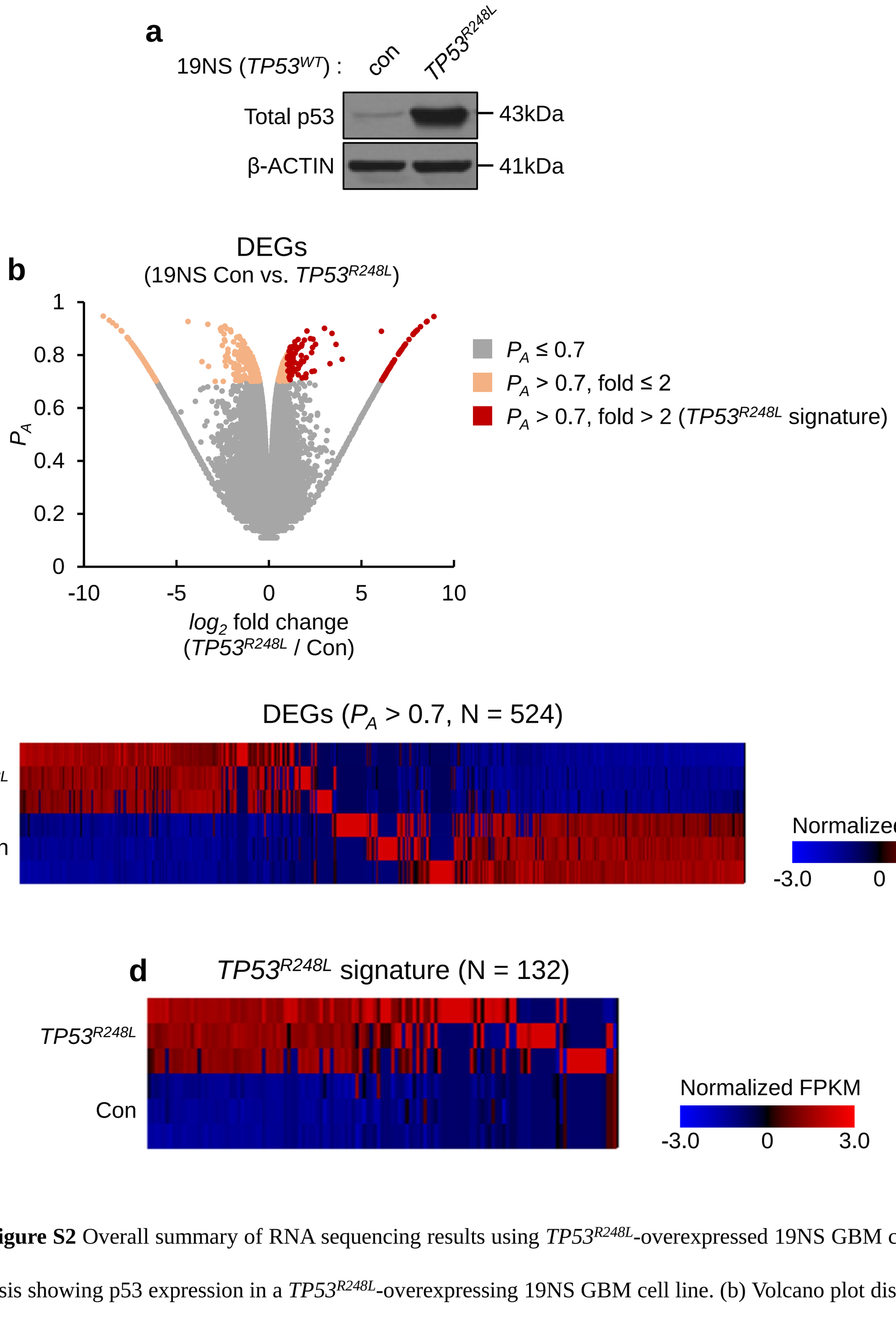

Supplementary Figure S2 Overall summary of RNA sequencing results using *TP53*^{R248L}-overexpressed 19NS GBM cell line. (a) Western blot analysis showing p53 expression in a *TP53*^{R248L}-overexpressing 19NS GBM cell line. (b) Volcano plot displaying P_A and $\log_2$ fold change of expression of differentially expressed genes (DEGs). (c) Heat map showing the expression of DEGs with P_A greater than 0.7. (d) Heat map showing the expression of *TP53*^{R248L} signature genes.

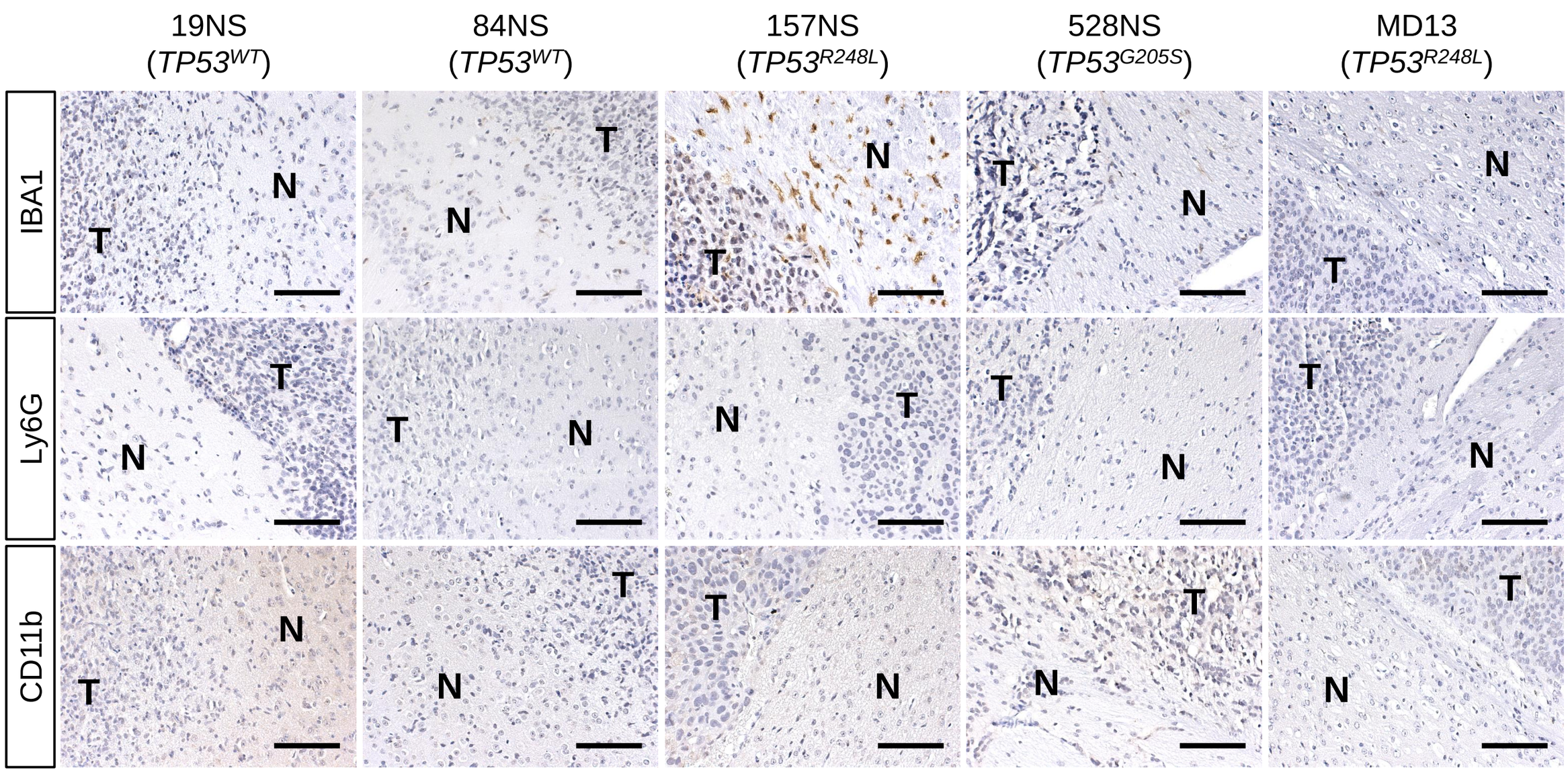

Supplementary Figure S3 IHC for immune cell markers in the normal brain regions adjacent to the patient-derived GBM xenograft tumors. We did not observe significant changes in the immune cell composition in the normal brain regions adjacent to the tumor, except for 157NS, which displayed increase in the number of IBA1^{+} cells. Representative microscopic images showing IHC positivity against IBA1, Ly6G, and CD11b in the normal brain region (N) adjacent to the tumor (T).

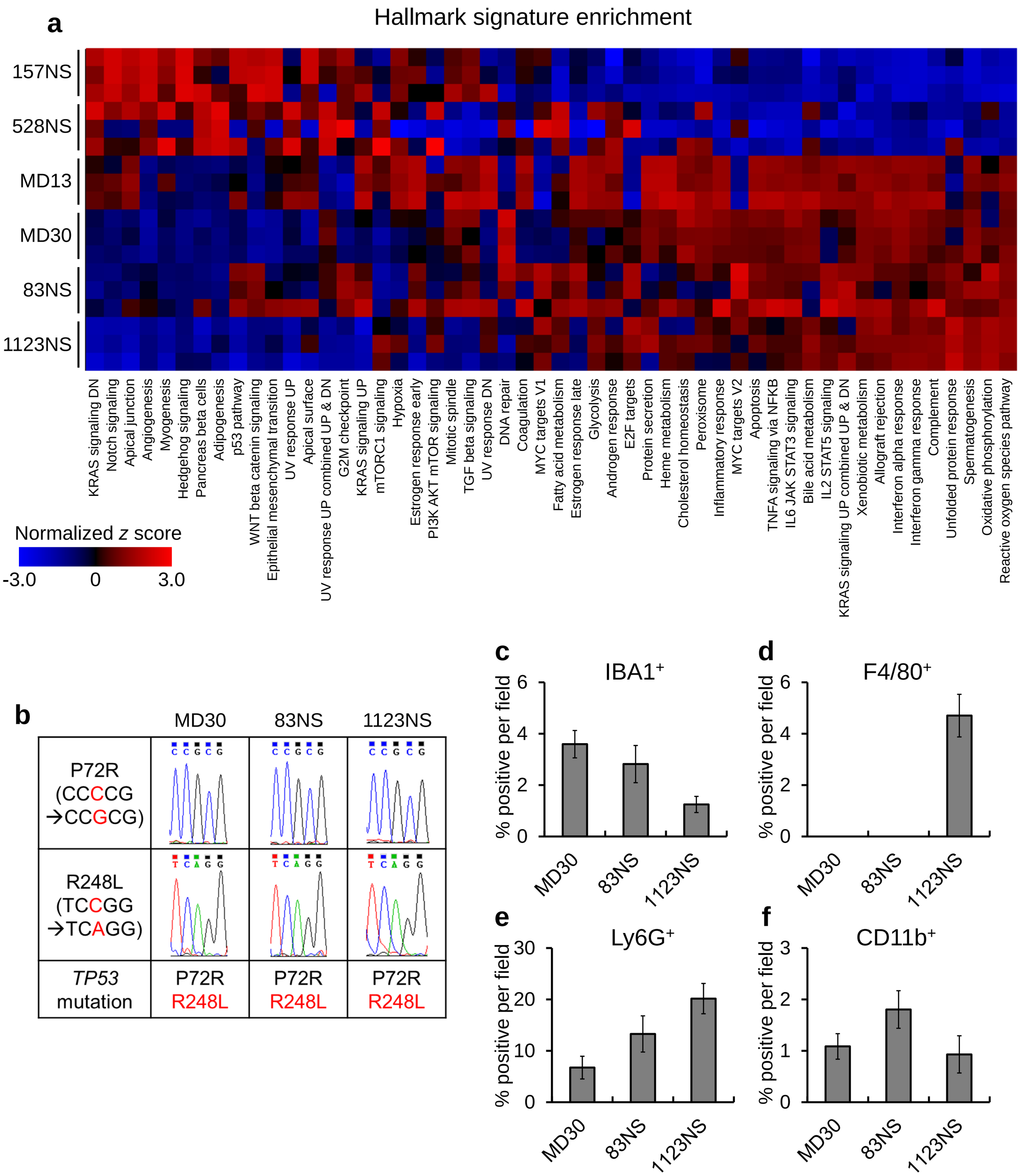

Supplementary Figure S4 IHC for immune cell markers in the patient-derived GBM xenograft tumors (*n* = 3). (a) Heat map demonstrating the ssGSEA result obtained using patient-derived GBM lines and hallmark signatures. (b) Nucleotide substitutions detected by *TP53* coding DNA sequence analysis. (c) Quantification of IHC for the composition of $IBA1^+$, $F4/80^+$ $Ly6G^+$, and $CD11b^+$ immune cells. The bar graph represents mean ± SEM.

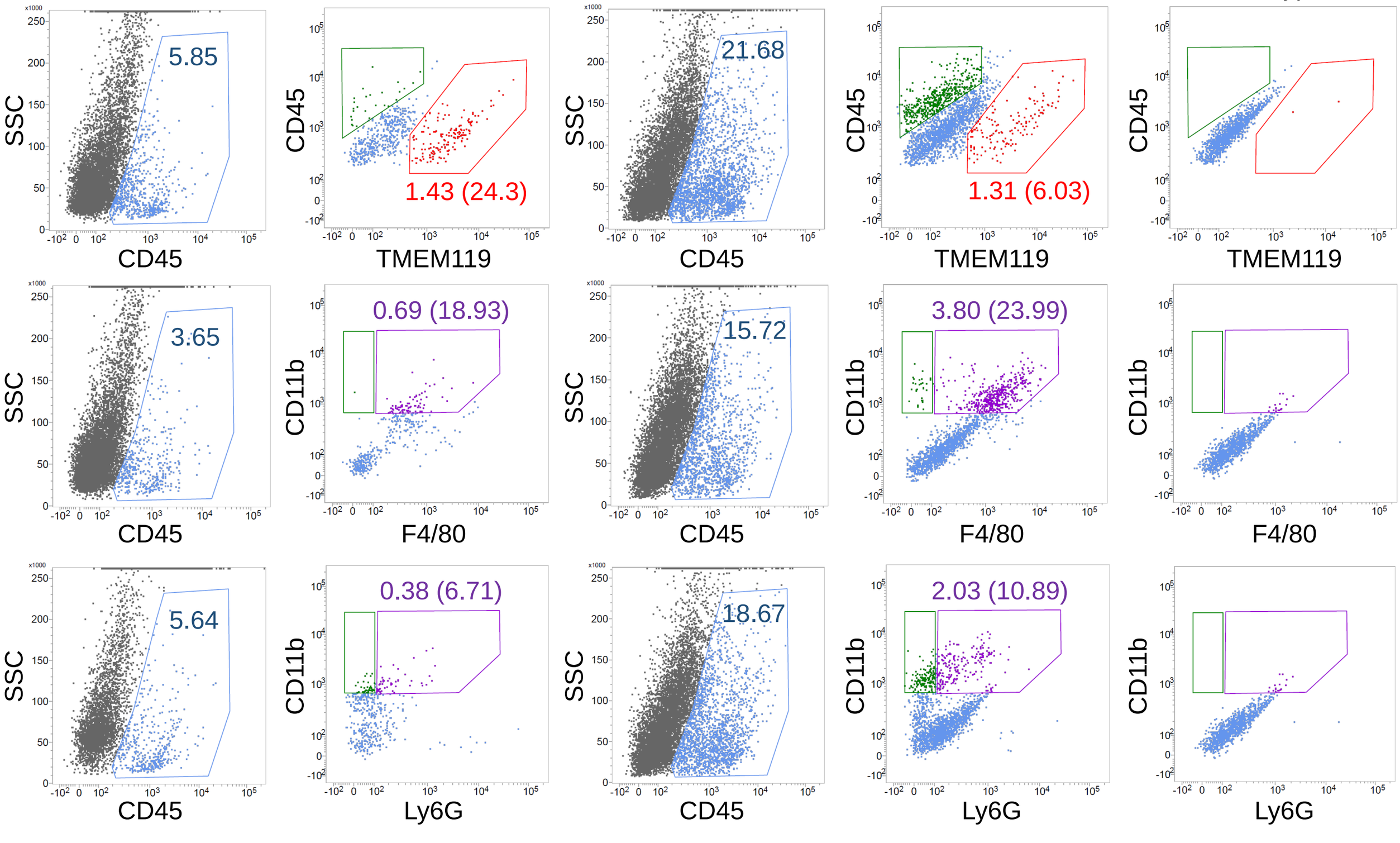

Supplementary Figure S5 Flow cytometry-mediated detection of immune cells in the MD13 xenograft tumor compared to the normal brain. Dot plots showing the result of flow cytometry for measuring the composition of microglia ($CD45^+/TMEM119^+$), macrophages ($CD45^+/CD11b^+/F4/80^+$), and neutrophils ($CD45^+/CD11b^+/Ly6G^+$) in the normal brain and MD13 xenograft brain tumor. Percentage values outside brackets indicate the ratio of each immune cell type to whole cells, whereas values inside brackets indicate the ratio to $CD45^+$ cells.

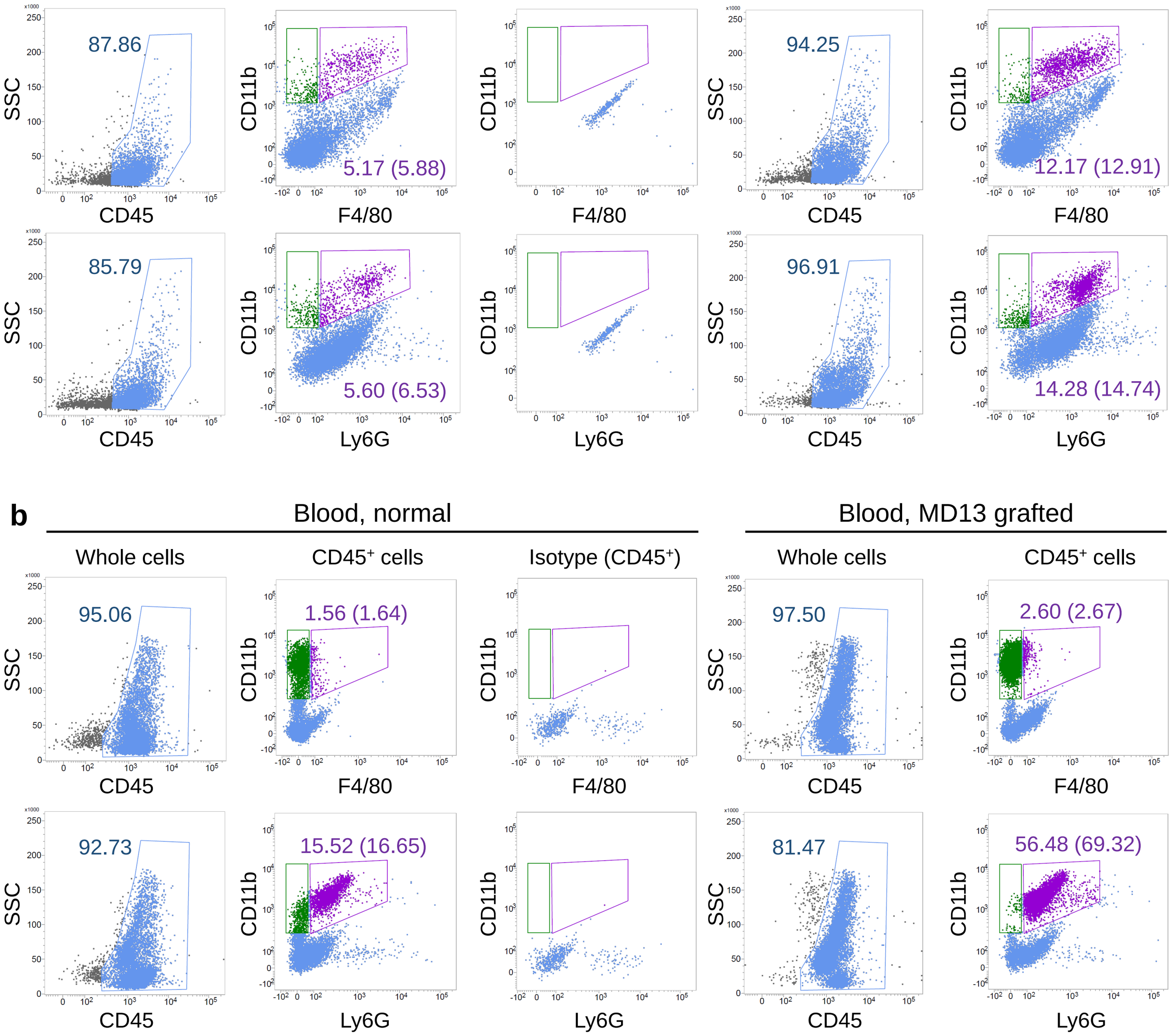

See the next page for the figure legend.

Supplementary Figure S6 Flow cytometry-mediated detection of immune cells in the circulation of MD13-grafted mice and normal mice. (a) Dot plots showing the result of flow cytometry for measuring the macrophage ($CD45^+/CD11b^+/F4/80^+$) and neutrophil ($CD45^+/CD11b^+/Ly6G^+$) composition of spleen. (b) Dot plots showing the macrophage and neutrophil composition of blood. In (a) and (b), percentage values outside brackets indicate the ratio of each immune cell type to whole cells, whereas values inside brackets indicate the ratio to $CD45^+$ cells. (c, d) Quantification of the flow cytometry result of (a) and (b), respectively. The bar graph represents mean ± SEM (**$P < 0.01$; ***$P < 0.001$; $n = 3$).

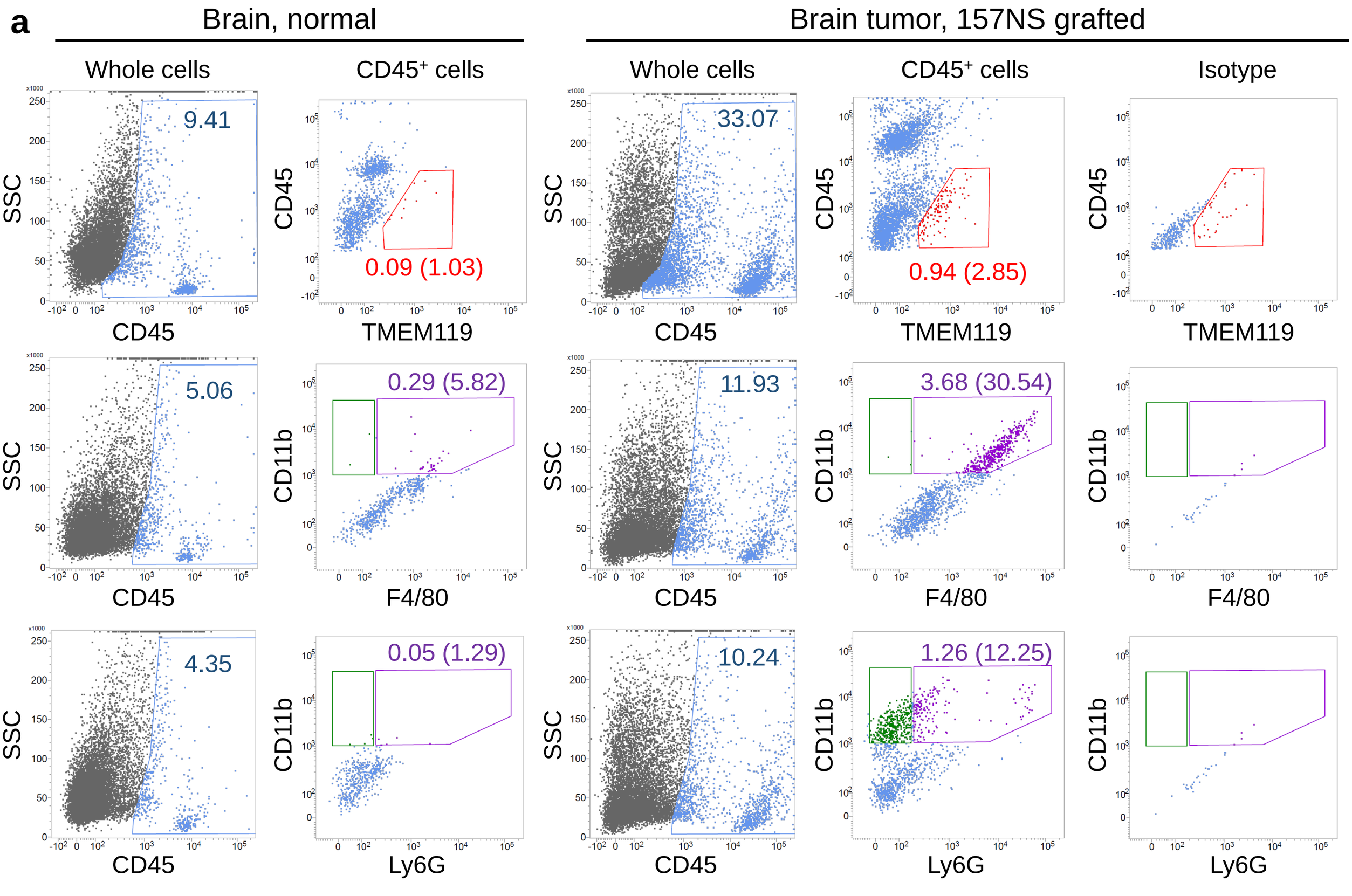

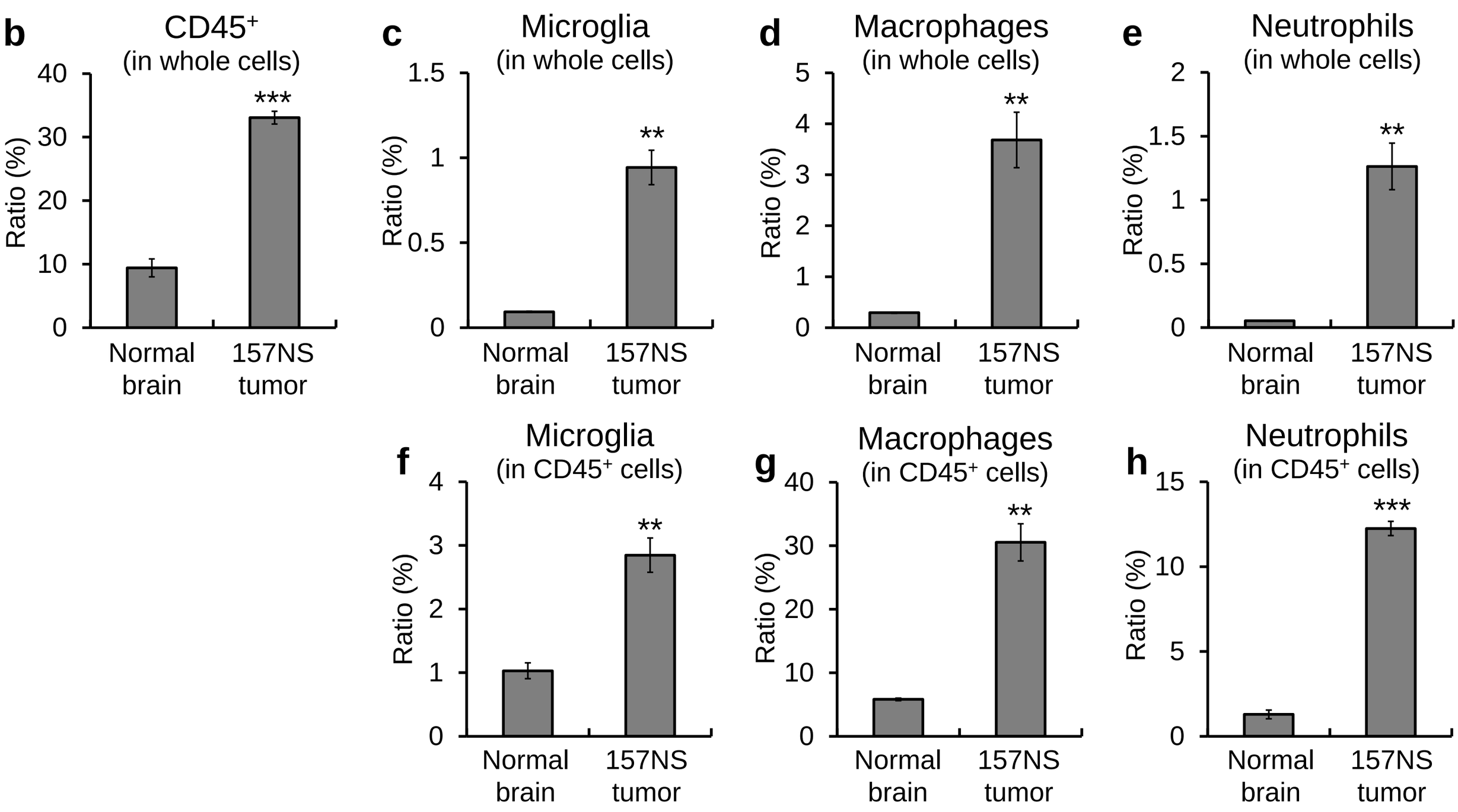

See the next page for the figure legend.

Supplementary Figure S7 Flow cytometry-mediated detection of immune cells in the 157NS xenograft tumor and normal brain. (a) Dot plots showing the result of flow cytometry for measuring the microglia ($CD45^+/TMEM119^+$), macrophage ($CD45^+/CD11b^+/F4/80^+$), and neutrophil ($CD45^+/CD11b^+/Ly6G^+$) composition of normal brain and 157NS xenograft brain tumor. Percentage values outside brackets indicate the ratio of each immune cell type to whole cells, whereas values inside brackets indicate the ratio to $CD45^+$ cells. (b-h) Quantification of flow cytometry results shown in (a). The bar graph represents mean ± SEM (**$P < 0.01$; ***$P < 0.001$; $n = 3$).

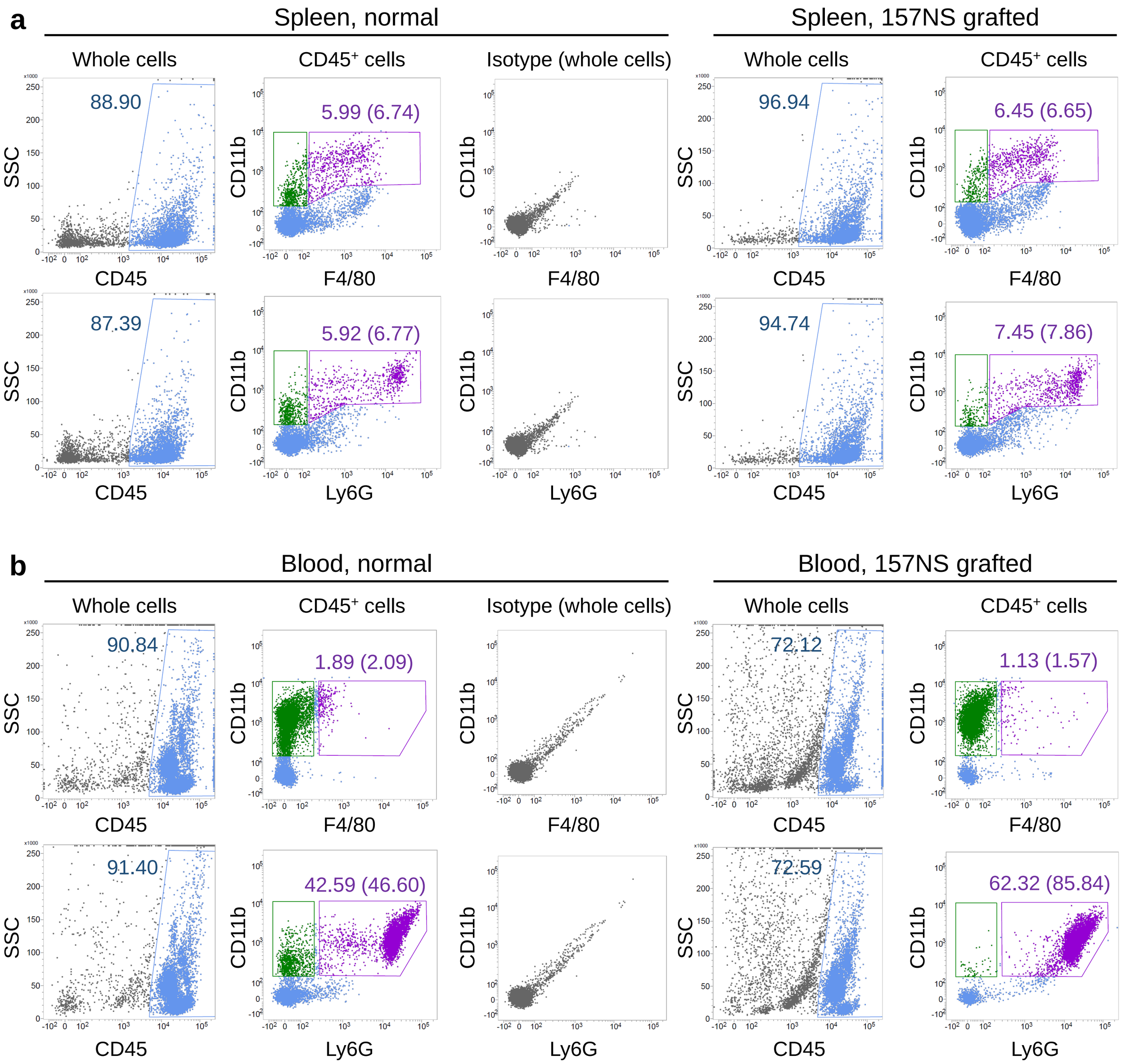

See the next page for the figure legend.

Supplementary Figure S8 Flow cytometry-mediated detection of immune cells in the circulation of 157NS-grafted mice and normal mice. (a) Dot plots showing the result of flow cytometry for measuring the macrophage ($CD45^+/CD11b^+/F4/80^+$) and neutrophil ($CD45^+/CD11b^+/Ly6G^+$) composition of spleen. (b) Dot plots showing the macrophage and neutrophil composition of blood. In (a) and (b), percentage values outside brackets indicate the ratio of each immune cell type to whole cells, whereas values inside brackets indicate the ratio to $CD45^+$ cells. (c, d) Quantification of flow cytometry results shown in (a) and (b), respectively. The bar graph represents mean ± SEM (**$P < 0.01$; ***$P < 0.001$; $n = 3$).

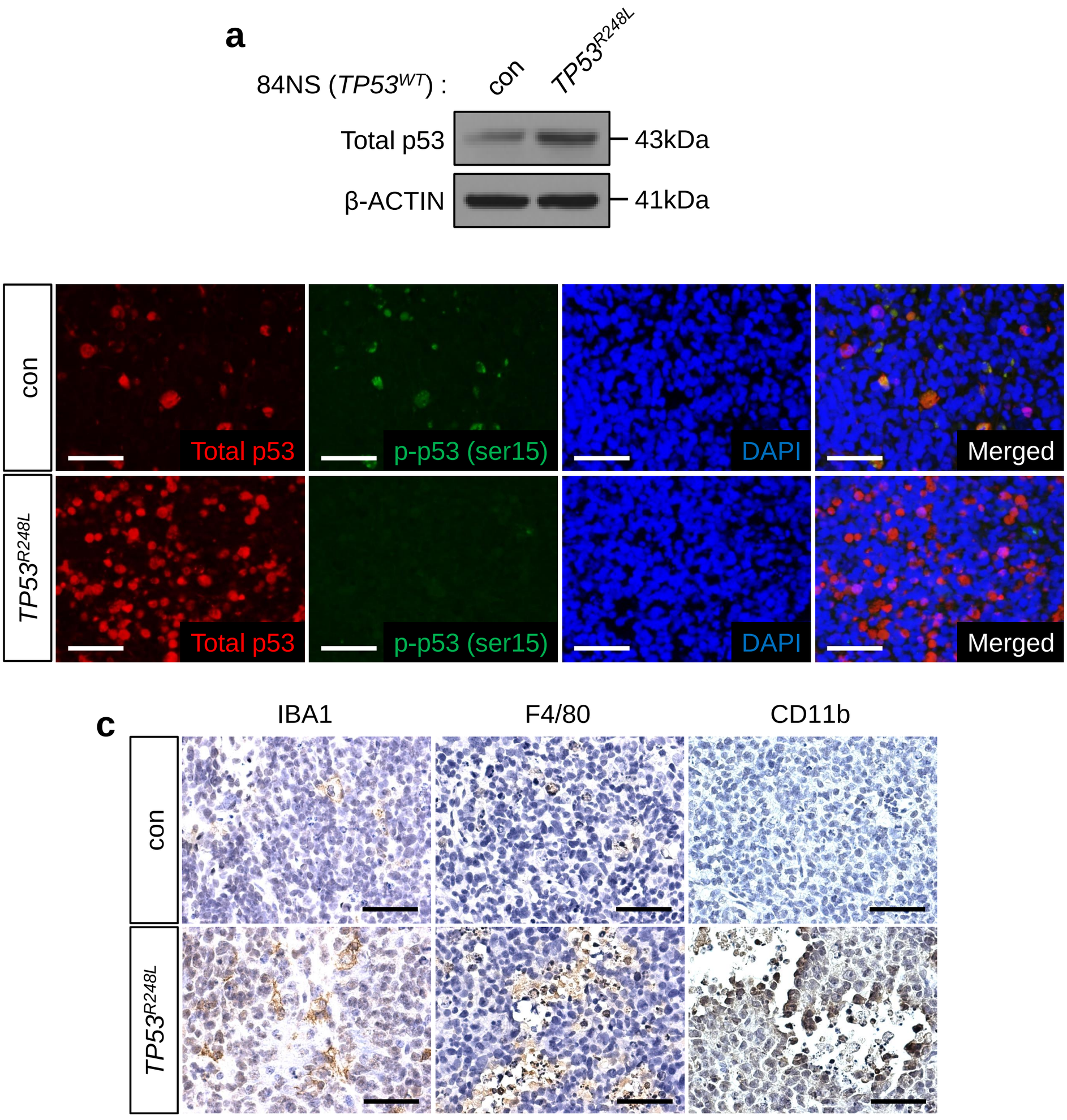

Supplementary Figure S9 Ectopic expression of *TP53*^{R248L} promotes immune cell infiltration. (a) Western blot analysis showing p53 overexpression in *TP53*^{R248L}-overexpressing 84NS cell line. (b) Representative microscopic images of fluorescent IHC showing total p53 and p-p53 (ser15) in orthotopically transplanted tumors generated using the *TP53*^{R248L}-overexpressing 84NS cell line. (c) Representative microscopic images of IHC for the expression of immune cell markers, including IBA1, F4/80, and CD11b. (d-f) Quantification of IHC showing the composition of IBA1$^+$, F4/80$^+$, and CD11b$^+$ cells. Representative microscopic images are magnified 400× (scale bar = 50 μm). The bar graph represents mean ± SEM (*$P < 0.05$; **$P < 0.01$).

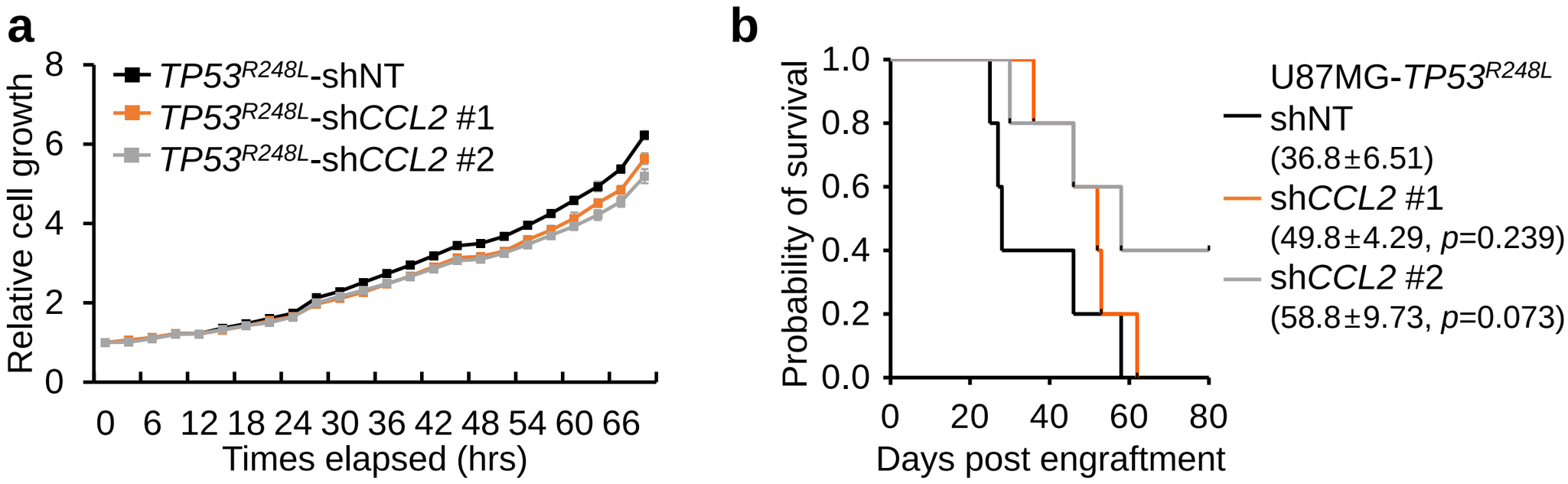

Supplementary Figure S10 Effect of *CCL2* knockdown on the growth of the *TP53*^{R248L}-expressing U87MG. (a) *In vitro* cell growth of the *TP53*^{R248L}-expressing U87MG with or without *CCL2* knockdown. (b) Kaplan-Meier survival plot showing survival of mice grafted with *TP53*^{R248L}-expressing U87MG with or without *CCL2* knockdown. *P*-values were calculated by log-rank t-test comparing the survival of sh*CCL2* #1 or sh*CCL2* #2 to shNT. Mean ± SEM of the overall survival of mice were calculated at the 80th day post-engraftment.

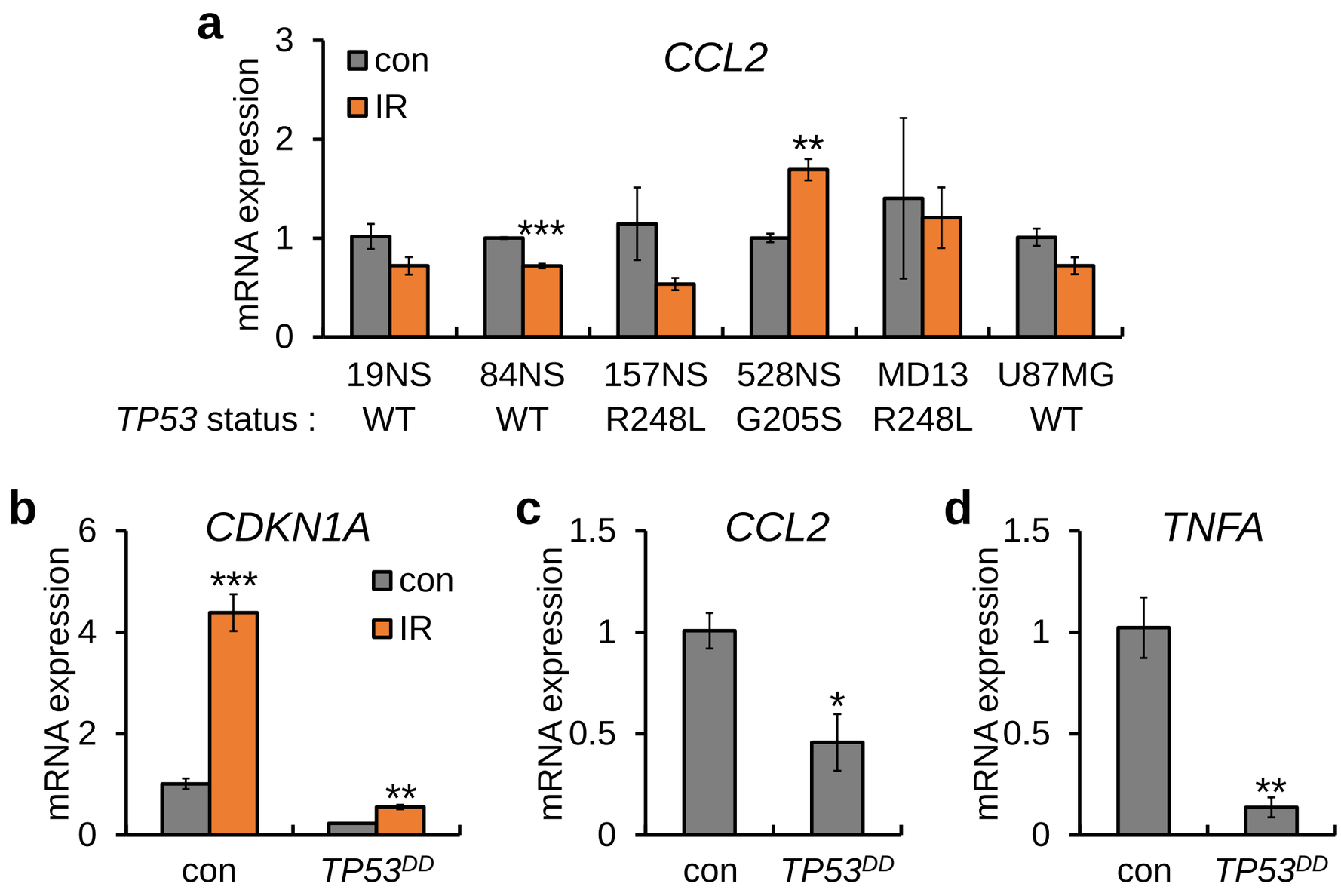

Supplementary Figure S11 *CCL2* and *TNFA* expression is not regulated by the dominant-negative function of mutant p53. (a) qPCR analysis showing *CCL2* mRNA level after 10 Gy IR treatment of the patient-derived GBM and U87MG cell lines. (b) qPCR analysis showing mRNA level of *CDKN1A* after 10 Gy IR treatment in $TP53^{DD}$-overexpressing U87MG cell line. (c, d) qPCR analysis showing mRNA levels of *CCL2* and *TNFA* in $TP53^{DD}$-overexpressing U87MG cell line. The bar graph represents mean ± SEM (**P* < 0.05; ***P* < 0.01; ****P* < 0.001; *n* = 3).

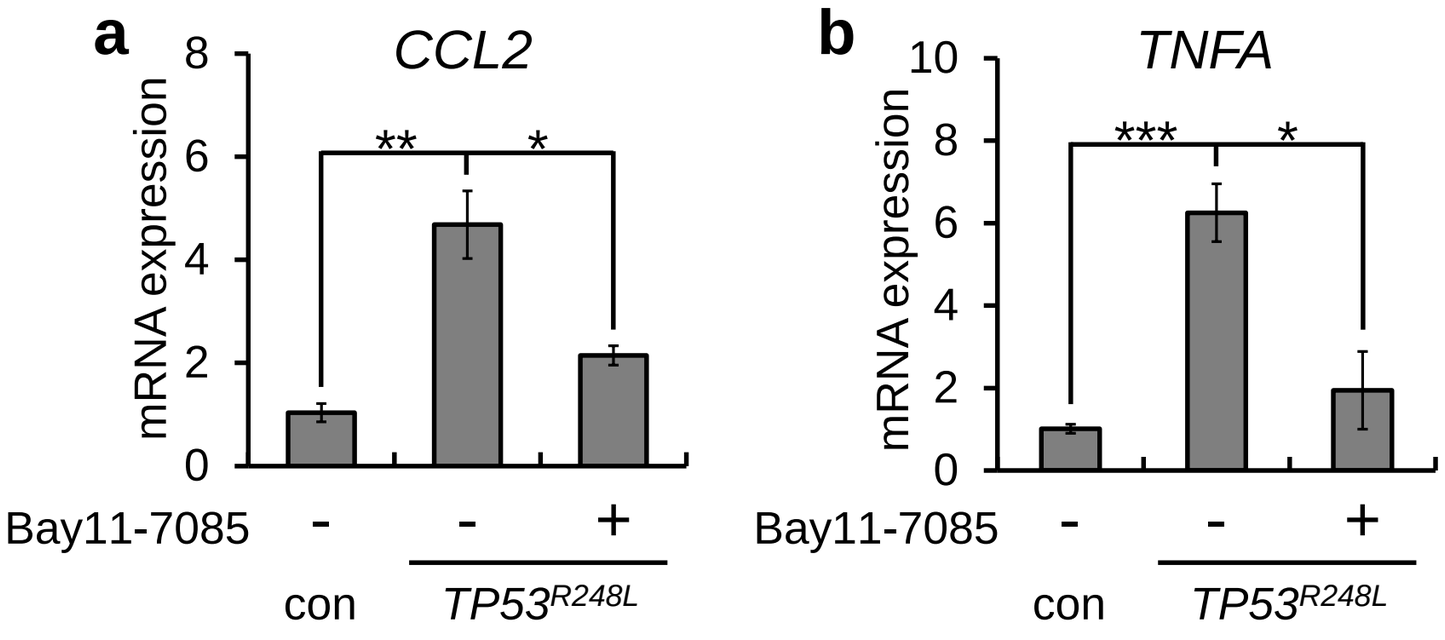

Supplementary Figure S12 NFκB inhibition blocks *TP53*^{R248L}-induced upregulation of *CCL2* and *TNFA*. (a, b) qPCR analysis showing mRNA levels of *CCL2* and *TNFA* after Bay 11-7085 treatment of the *TP53*^{R248L}-overexpressing U87MG cell line. The bar graph represents mean ± SEM (*$P < 0.05$; **$P < 0.01$; ***$P < 0.001$; $n = 3$).

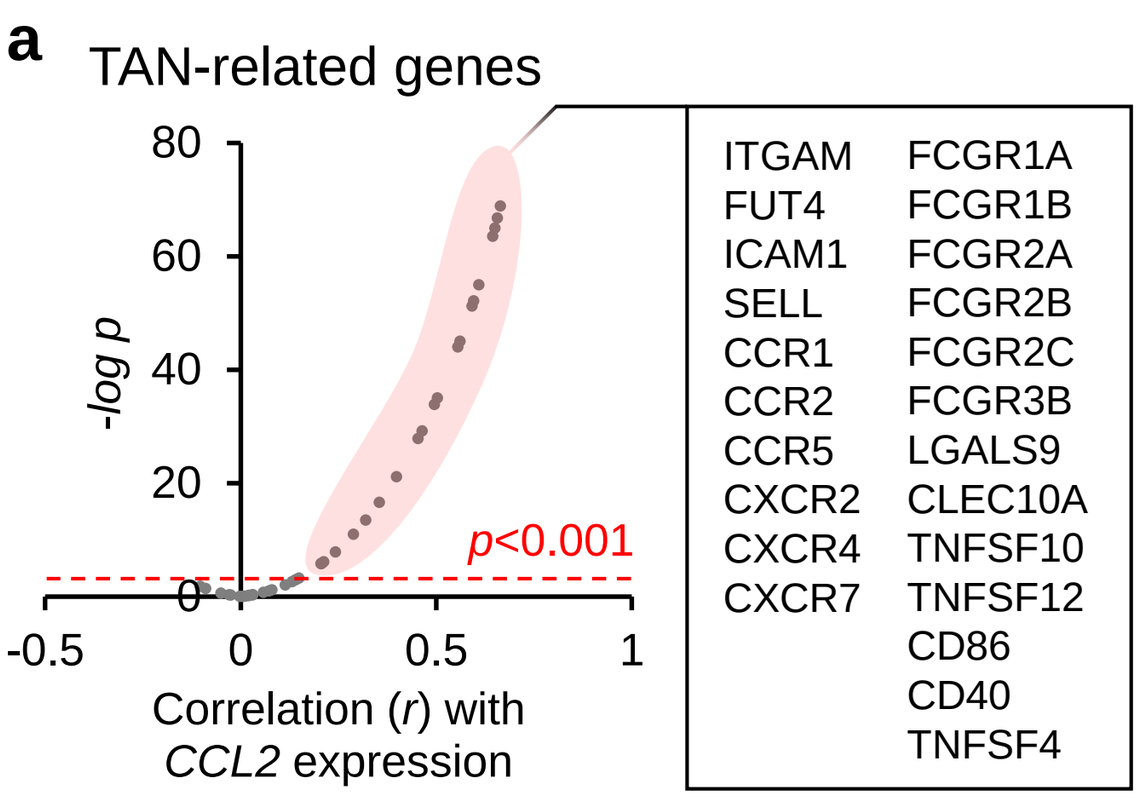

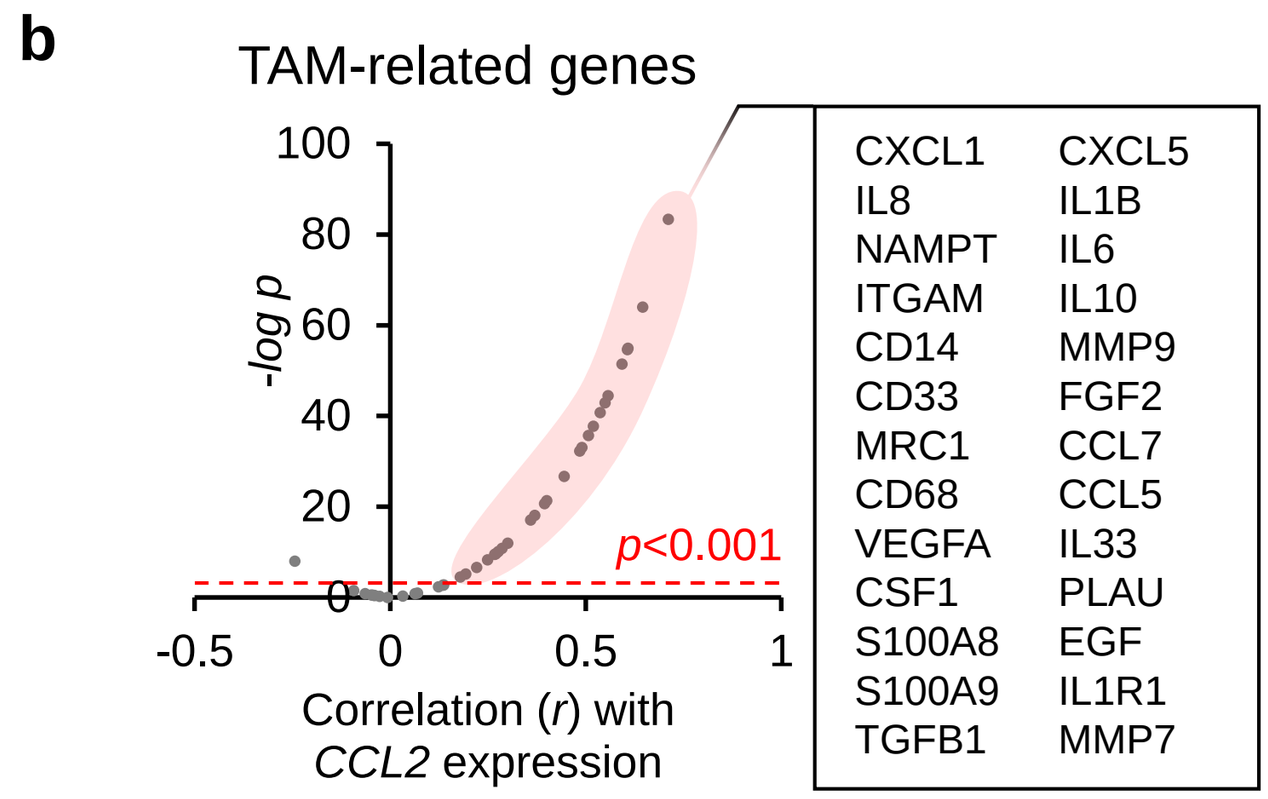

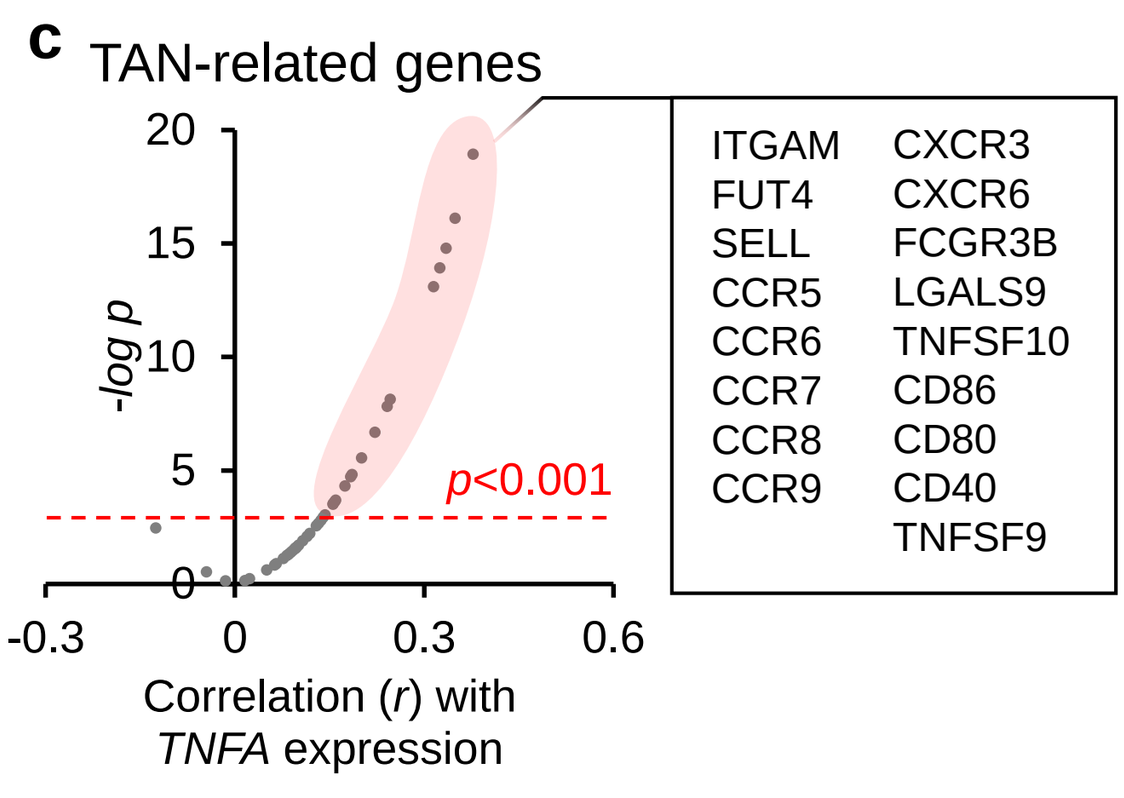

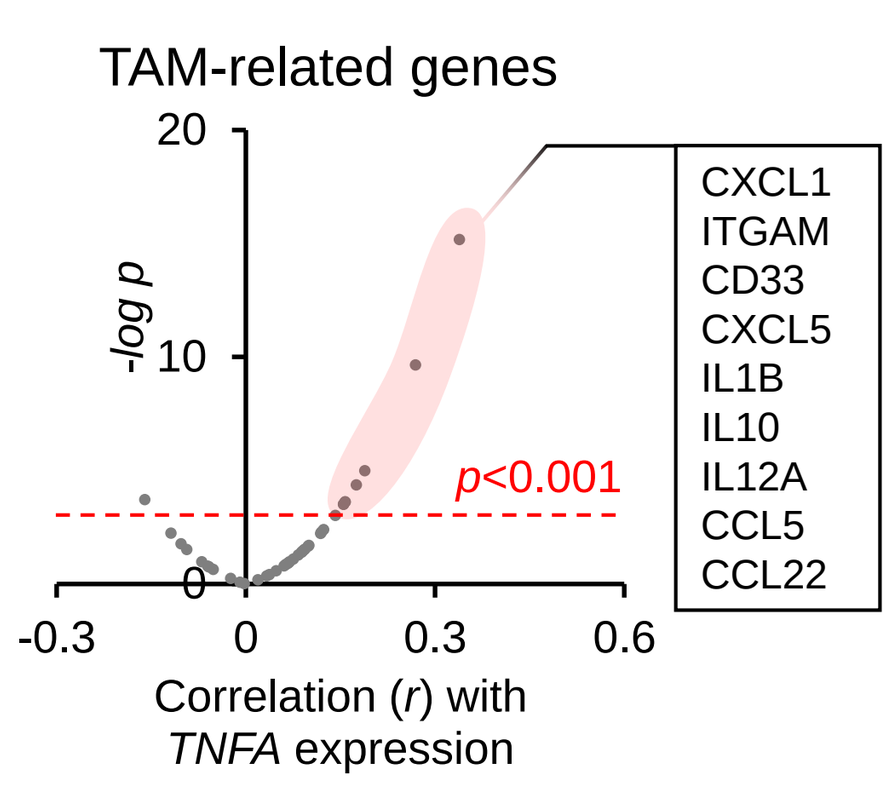

Supplementary Figure S13 *CCL2* and *TNFA* are positively correlated with TAN- and TAM-related genes. (a, b) Correlations between *CCL2* expression and expression of TAN- and TAM-related genes, respectively. (c, d) Correlations between *TNFA* expression and expression of TAN- and TAM-related genes, respectively. All analyses show data obtained using the TCGA GBM patient gene set.

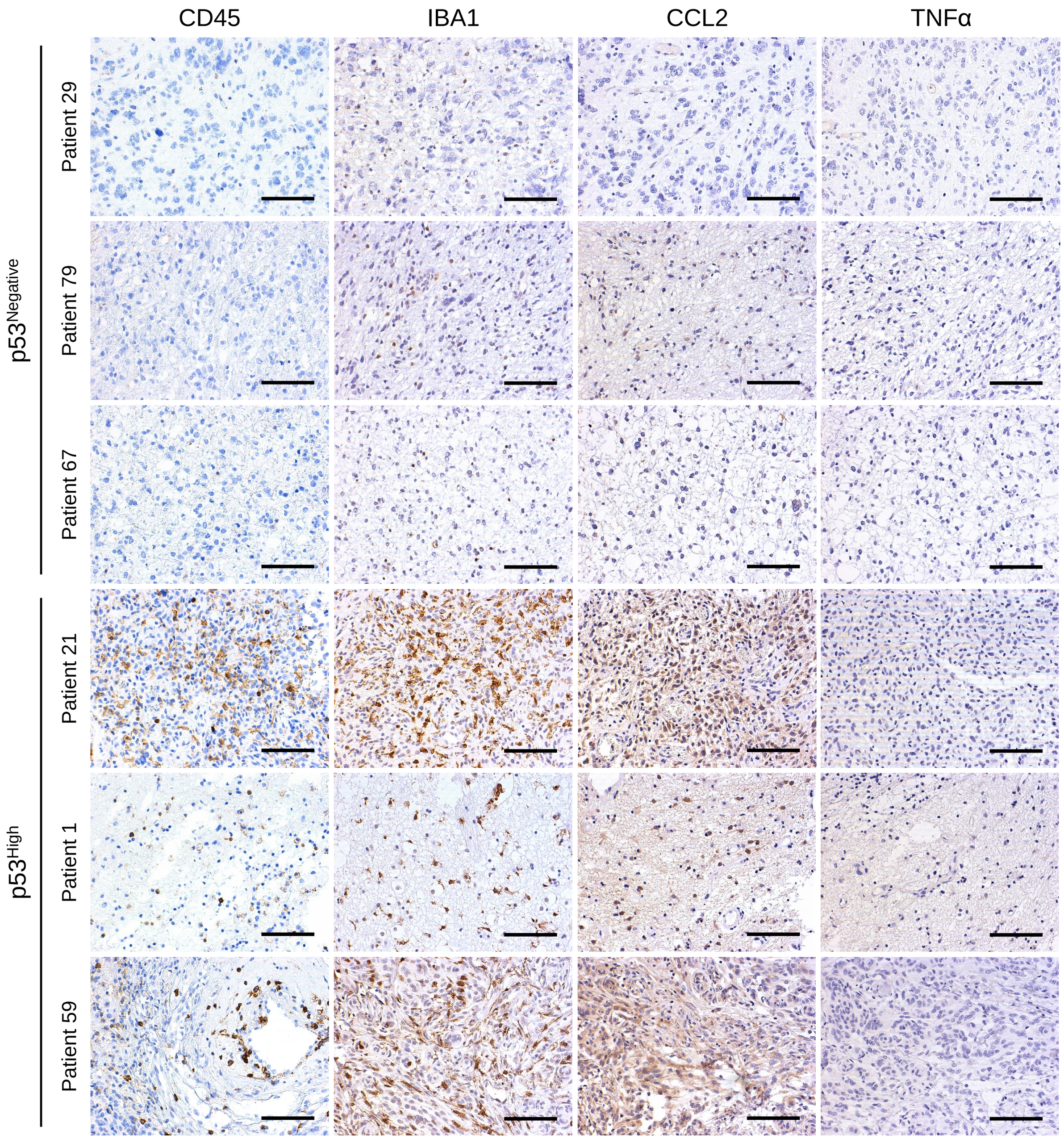

Supplementary Figure S14 Representative microscopic images of IHC using the patient GBM specimens. The microscopic images have been magnified 200× (scale bar = 100 μm).

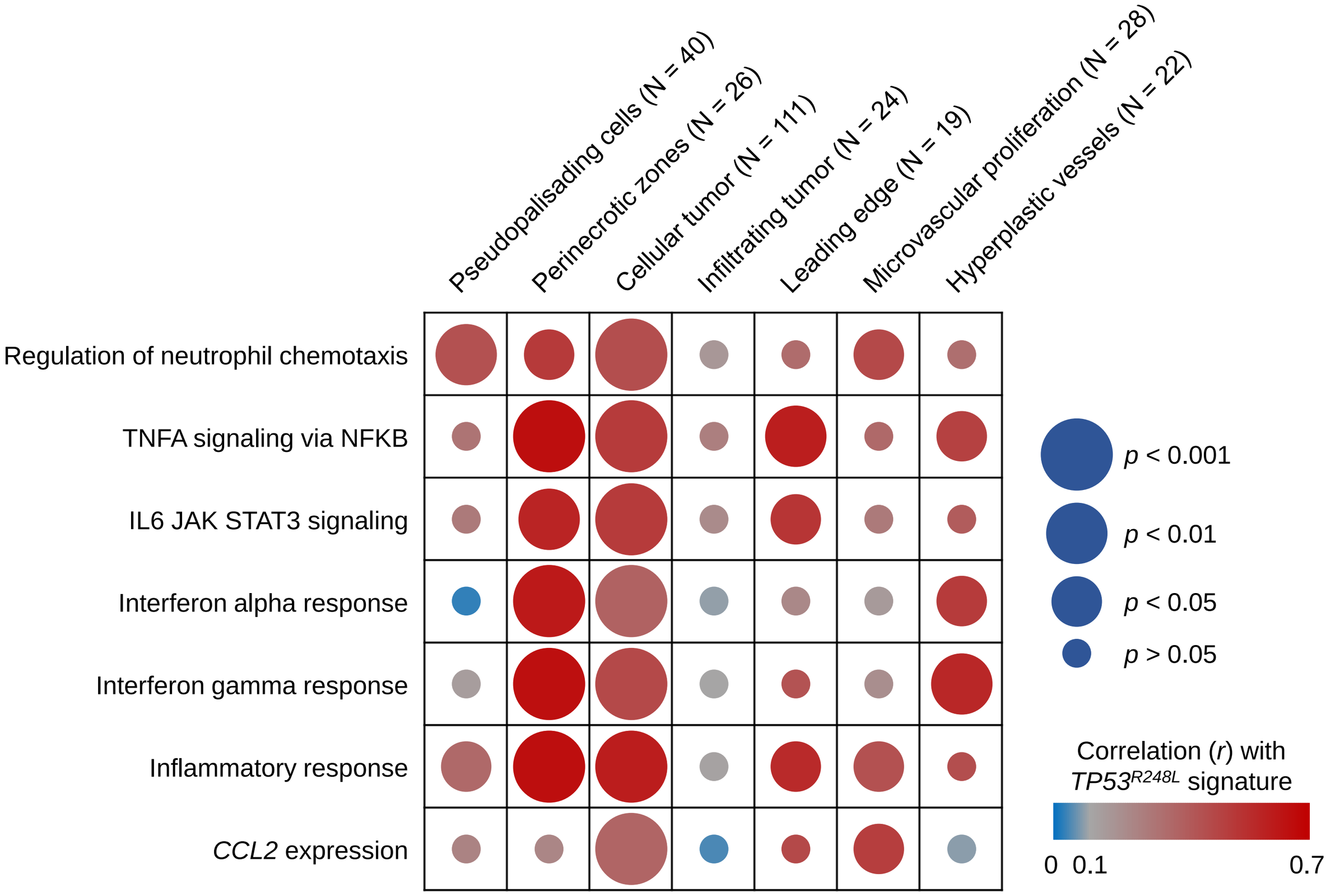

Supplementary Figure S15 Inflammation-related signatures and *CCL2* expression correlate with *TP53*^{R248L} signature, depending on the sub-tumor localization. A correlation plot demonstrating the correlation between *TP53*^{R248L} signature, and inflammation-related signatures or *CCL2* expression, in the patient tissue RNA sequencing data from IVY GAP. Circle color indicates the correlation coefficient (*r*), whereas size denotes the *P* value determined by t-test.

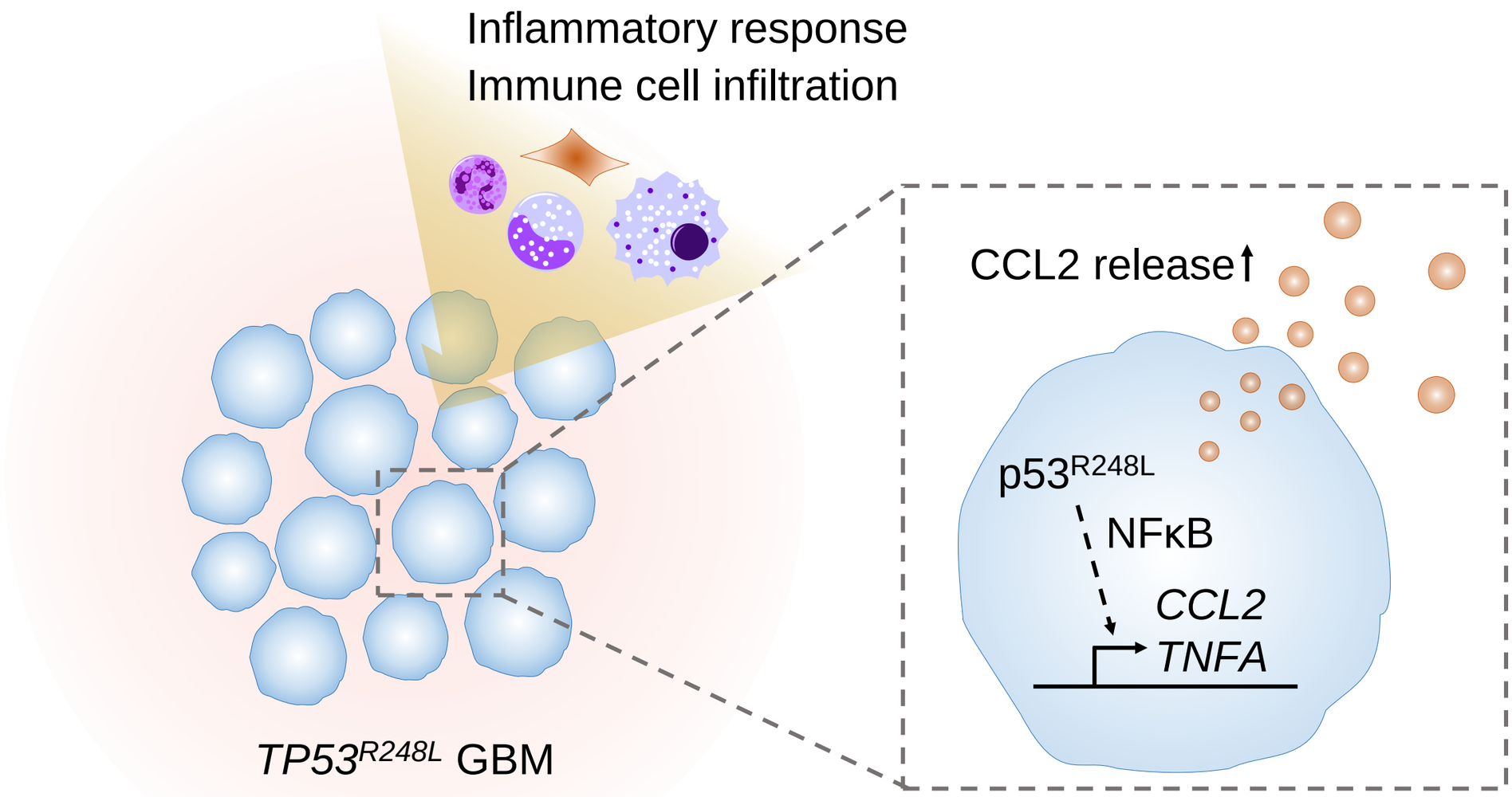

Supplementary Figure S16 Graphic summary showing our hypothesis. *TP53*^{R248L} promotes inflammatory responses and increase in immune cell infiltration. As an underlying mechanism, p53^{R248L} upregulates *CCL2* and *TNFA* expression via NFκB signaling.